# First-principles calculation of the Dzyaloshinskii-Moriya interaction: A Green's function approach

Farzad Mahfouzi \* and Nicholas Kioussis \*

Department of Physics and Astronomy, California State University, Northridge, California 91330-8268, USA

(Received 23 December 2020; revised 1 February 2021; accepted 24 February 2021; published 5 March 2021)

We present a Green's function approach to calculate the Dzyaloshinskii-Moriya interactions (DMIs) from first-principles electronic structure calculations that is computationally more efficient and accurate than the most commonly employed supercell and generalized Bloch-based approaches. The method is applied to the (111) Co/Pt bilayer where the Co and/or Pt thickness dependence of the DMI coefficients is calculated. Overall, the calculated DMIs are in relatively good agreement with the corresponding values reported experimentally. Furthermore, we investigate the effect of strain in the DMI tensor elements and show that the isotropic Néel DMI can be significantly modulated by the normal strains  $\epsilon_{xx}$  and  $\epsilon_{yy}$  and is relatively insensitive to the shear strain  $\epsilon_{xy}$ . Moreover, we show that anisotropic strains,  $(\epsilon_{xx} - \epsilon_{yy})$  and  $\epsilon_{xy}$ , result in the emergence of anisotropic Néel- and Bloch-type DMIs, respectively.

DOI: 10.1103/PhysRevB.103.094410

#### I. INTRODUCTION

Magnetic skyrmions [1–5] are noncollinear spin configurations found in materials with strong spin-orbit coupling (SOC) and noncentrosymmetric crystal structures which lack an inversion center. Their existence was theoretically predicted three decades ago [4,5] and experimentally observed recently in chiral magnets and other B20-type bulk materials, such as MnSi [6], Fe<sub>1-x</sub>Co<sub>x</sub>Si [7], FeGe [8], and  $Mn_{1-x}Fe_xGe$  [9]. Bilayer devices consisting of ferromagnets interfaced with heavy metals, with their mirror symmetry broken across the interface, also provide the necessary condition for the emergence of skyrmions [10–19]. The noncollinearity of the spin configuration is conventionally parameterized by the Dzyaloshinskii-Moriya interaction (DMI) [20,21], an antisymmetric exchange interaction between atomic magnetic moments, which is generally measured experimentally using Brillouin light scattering (BLS) [22-28]. The DMI energy for two spins,  $\vec{S}_1$  and  $\vec{S}_2$ , separated by a distance  $\vec{R}$  is of the form  $E_{\rm DMI} = \vec{d}_{\vec{R}} \cdot (\vec{S}_1 \times \vec{S}_2)$  [20,21], where the DMI vector generally consists of two terms [29], referred to as the Bloch,  $\vec{d}^B$ , and Néel,  $\vec{d}^N$ , components, respectively. In metallic systems the DMI is mediated by the conduction electrons. Conduction electrons with spin-momentum coupling of the Rashba type are known to lead to a Néel DMI [30-33]. This type of helicity is often present at the interface between two different materials, where the broken inversion symmetry normal to the interface results in a DMI vector of the form  $\vec{d}^N = d^N \vec{e}_z \times \vec{R}/|\vec{R}|$ , where  $\vec{e}_z$  is the unit vector normal to the interface. On the other hand, systems with Dresselhaus-type SOC, which is often manifested in the bulk region, exhibit a Bloch-type DMI vector [6,7,34] of the form  $\vec{d}^B = -d^B \vec{R}/|\vec{R}|$ .

Magnetic skyrmions are promising candidates for several applications [35], including racetrack memory [36–38], skyrmion-based logic gates [39], microwave devices [40], and neuromorphic computing [41,42]. Such devices require efficient ways of skyrmion manipulation [17,43-47], including creation, annihilation, motion, and detection. Interestingly, recent experiments have demonstrated the electric field- [48–50] and/or strain-mediated [51] modulation of the interfacial DMI which may provide a novel function for skyrmion- or chiraldomain-wall-based spintronic devices. However, in order for the skyrmion nucleation to be energetically feasible and stable at room temperature, large DMI values are required [19,52– 54], making it difficult to significantly modulate the sign and/or amplitude of the DMI. To address this issue, firstprinciples calculations provide a promising avenue in the search for devices with large DMI that are also responsive to external perturbations.

Several first-principles approaches have so far been introduced to calculate the DMI. These include the supercell [55], the generalized Bloch theorem [56], the Korringa-Kohn-Rostoker Green's function (KKR-GF) [57], and the Berry curvature [58] methods. Even though the supercell approach to evaluate the DMI from first principles is the most common, it is computationally demanding and hence limits its application to systems with a small number of atoms. The generalized Bloch theorem approach is computationally less demanding than the supercell, albeit at the cost of taking into account the effect of SOC perturbatively. On the other hand, the KKR-GF and Berry curvature methods are computationally the most efficient while taking into account the effect of SOC exactly.

Developing an accurate and efficient first-principles approach to calculate the DMI and its manipulation via current [59], electric field [60], and strain [61,62] is of paramount importance in the spintronics community. In this paper, we employ the Green's function method to calculate the atomistic exchange coupling from the magnon band structure in the spin-spiral regime. The DMIs are calculated for the Pt/Co

<sup>\*</sup>Farzad.Mahfouzi@gmail.com

<sup>†</sup>nick.kioussis@csun.edu

bilayer for various Pt and/or Co thicknesses and are compared with the corresponding values reported in experiments, where the overall agreement is good. Furthermore, we have investigated the effect of strain on the DMI tensor elements, which is in relative agreement with the recent experimental observation [51].

### II. THEORETICAL FORMALISM

#### A. Phenomenological modeling

Investigations of magnetic properties of materials at the phenomenological level based on model spin Hamiltonians may be formulated either in the continuum (micromagnetic) or in the discrete atomistic representation.

The Hamiltonian governing the atomic spin dynamics can be generally written as

$$E_M = -\frac{1}{2} \sum_{ij:\vec{R}\vec{R}':\alpha\beta} J_{\vec{R}-\vec{R}'}^{ij,\alpha\beta} \vec{m}_{\vec{R}}^i \cdot \vec{e}_{\alpha} \vec{m}_{\vec{R}'}^j \cdot \vec{e}_{\beta}, \tag{1}$$

where  $\vec{m}_{\vec{R}}^{i(j)}$  is a unit vector along the local magnetic moment of the *i*th (*j*th) atom within the unit cell at  $\vec{R}$  ( $\vec{R}'$ ),  $J_{\vec{R}-\vec{R}'}^{ij,\alpha\beta}$  is the relativistic exchange coupling between the two local moments, and  $\vec{e}_{\alpha}$  is a unit vector along the  $\alpha=x,y,z$  direction.

The Landau-Lifshitz equation of motion is then given by

$$\frac{M_i}{2\mu_B} \frac{\partial}{\partial t} \vec{m}_{\vec{R}}^i = \vec{m}_{\vec{R}}^i \times [\hat{J}\vec{m}]_{\vec{R}}^i, \tag{2a}$$

$$[\hat{J}\vec{m}]_{\vec{R}}^{i} \cdot \vec{e}_{\alpha} = \sum_{\vec{p}', i\beta} J_{\vec{R}-\vec{R}'}^{ij,\alpha\beta} \vec{m}_{\vec{R}'}^{j} \cdot \vec{e}_{\beta}, \tag{2b}$$

where  $M_i$  is the magnetic moment of the *i*th atom. In the linear regime the time-dependent local moment direction can be written as

$$\vec{m}_{\vec{p}}^{i}(t) \approx \vec{e}_z + \delta_{\vec{p}}^{i,x}(t)\vec{e}_x + \delta_{\vec{p}}^{i,y}(t)\vec{e}_y, \tag{3}$$

where, for simplicity, we choose  $\vec{e}_z$  as the direction around which the magnetization is precessing. A generalization of the approach to any given equilibrium magnetization direction is straightforward.

In the "spin spiral" regime we ignore the independent dynamics of magnetic moments within the unit cell, where the equations of motion in momentum space are given by

$$\frac{M_{\text{tot}}}{2\mu_B} \frac{\partial \delta_{\vec{q}}^x}{\partial t} = -J_{\vec{q}}^{yx} \delta_{\vec{q}}^x - (J_{\vec{q}}^{yy} - J_0^{zz}) \delta_{\vec{q}}^y, \tag{4a}$$

$$\frac{M_{\text{tot}}}{2\mu_B} \frac{\partial \delta_{\vec{q}}^y}{\partial t} = J_{\vec{q}}^{xy} \delta_{\vec{q}}^y + \left(J_{\vec{q}}^{xx} - J_0^{zz}\right) \delta_{\vec{q}}^x. \tag{4b}$$

Here,  $M_{\text{tot}} = \sum_{i} M_{i}$  is the total magnetic moment per unit cell and

$$J_{\vec{q}}^{\alpha\beta} = \sum_{ij,\vec{R}} J_{\vec{R}}^{ij,\alpha\beta} e^{i(\vec{r}_i - \vec{r}_j + \vec{R}) \cdot \vec{q}}.$$
 (5)

We can, in turn, make a connection between the parameters of the continuum model and the micromagnetic energy

defined as

$$E_{M} = \sum_{\alpha\beta} \int d^{3}\vec{R} \left[ A_{\alpha\beta} \frac{\partial m^{\alpha}}{\partial R_{\beta}} \frac{\partial m^{\alpha}}{\partial R_{\beta}} + K_{\alpha\beta} m^{\alpha} m^{\beta} + D_{\alpha\beta} \left( \vec{m} \times \frac{\partial \vec{m}}{\partial R_{\alpha}} \right) \cdot \vec{e}_{\beta} \right], \tag{6}$$

where  $A_{\alpha\beta}$ ,  $K_{\alpha\beta}$ , and  $D_{\alpha\beta}$  are the exchange stiffness, magnetocrystalline anisotropy (MCA), and DMI tensor elements, respectively. In this case the dynamical equations of motion are given by

$$\frac{M_{\text{tot}}}{4\mu_B V_M} \frac{\partial \vec{m}}{\partial t} = \sum_{\alpha\beta} \vec{m} \times \left( -A_{\alpha\beta} \frac{\partial^2 \vec{m}}{\partial R_{\alpha} \partial R_{\beta}} + K_{\alpha\beta} \vec{e}_{\alpha} m^{\beta} + D_{\alpha\beta} \frac{\partial \vec{m}}{\partial R_{\beta}} \times \vec{e}_{\alpha} \right). \tag{7}$$

Comparison of the linearized equation (7) with the system of equations (4) yields

$$K_{\alpha\beta} = \frac{1}{2V_M} J_{\vec{q}}^{\alpha\beta} \bigg|_{\vec{q}=\Gamma},\tag{8a}$$

$$D_{\alpha\beta} = \frac{1}{4V_M} Im \left( \sum_{\gamma\gamma'} \epsilon_{\beta\gamma\gamma'} \frac{\partial J_{\vec{q}}^{\gamma\gamma'}}{\partial q_{\alpha}} \right) \bigg|_{\vec{q}=\Gamma}, \tag{8b}$$

$$A_{\alpha\beta} = \frac{1}{2V_M} \frac{\partial^2 J_{\vec{q}}^{\alpha\alpha}}{\partial q_{\beta}^2} \bigg|_{\vec{q} = \Gamma}.$$
 (8c)

Here, the Levi-Civita symbol,  $\epsilon_{\alpha\beta\gamma}$ , is introduced to convert the third-order DMI tensor in Lifshitz invariant presentation [63] to a second-order tensor, and  $V_M$  is the volume of the unit cell of the ferromagnetic film. Equation (8b) can be used to calculate the DMI tensor elements  $D_{\alpha\beta}$ . However, consistent with the BLS method employed in experiments, in our first-principles calculations we use the magnon dispersion method to evaluate the different DMI components.

In the following we provide a phenomenological treatment of the DMI. This can be achieved by extending the Néel,  $\vec{d}^N$ , and Bloch,  $\vec{d}^B$ , components of the DMI vector for a pair of magnetic moments to a lattice of magnetic ions; the DMI tensor elements for a ferromagnetic/heavy-metal bilayer with broken mirror symmetry along the Cartesian z axis are given by

$$D_{\alpha\beta} = \frac{1}{2V_M} \sum_{\vec{R}} \left[ d_{\vec{R}}^N \frac{\vec{e}_z \times \vec{R}}{|\vec{R}|} + d_{\vec{R}}^B \frac{\vec{R}}{|\vec{R}|} \right] \cdot \vec{e}_\alpha R_\beta. \tag{9}$$

For an isotropic system, where the interatomic DMI coupling depends only on  $|\vec{R}|$ , the Néel and Bloch components of the DMI tensor result in the off-diagonal and diagonal matrix elements, respectively,

$$D_{\alpha\beta}^{\rm iso} = D^N \vec{e}_z \cdot \vec{e}_\alpha \times \vec{e}_\beta + D^B \vec{e}_\alpha \cdot \vec{e}_\beta, \tag{10}$$

where  $D^N = \sum_n N_n R_n d_n^N / 4V_M$  and  $D^B = \sum_n N_n R_n d_n^B / 4V_M$  and  $N_n$  denotes the number of nearest neighbors of the  $n_{\rm th}$  shell. For example, for a film with in-plane hexagonal crystal structure we have  $(R_n/a)^2 = (1, 3, 4, 7, 9, \dots)$  and  $N_n = (6, 6, 6, 12, 6, \dots)$ .

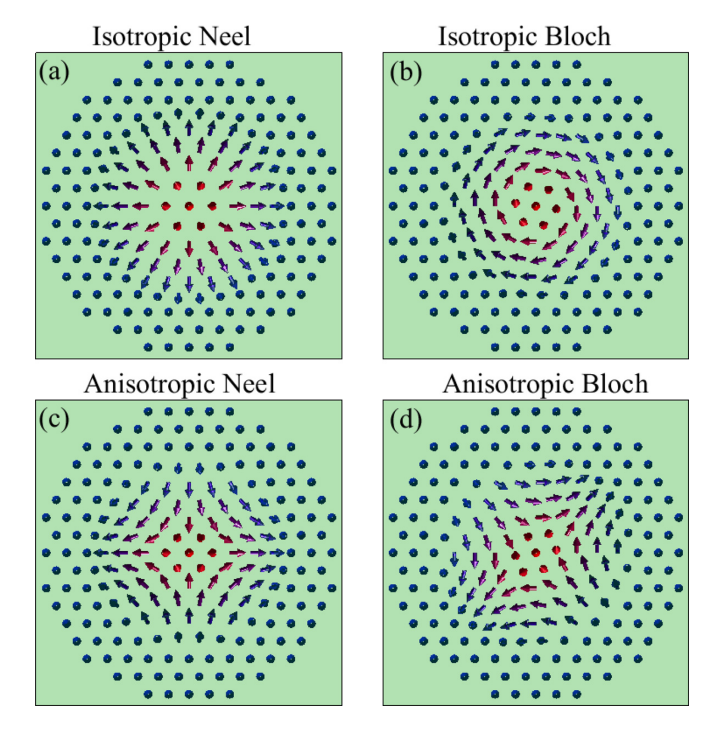


FIG. 1. Schematic spin texture for skyrmions resulting from isotropic (a) Néel and (b) Bloch DMI tensor components and antiskyrmions originating from anisotropic (c)Néel and (d) Bloch DMI tensor components. Red (blue) arrows denote the direction of the local magnetic moment along the  $+\vec{e}_{\tau}$  ( $-\vec{e}_{\tau}$ ) direction.

On the other hand, for an anisotropic system, the diagonal elements  $D_{\alpha\alpha}$  of the DMI matrix are not necessarily identical, and the off-diagonal elements (apart from the antisymmetric Néel component) can additionally acquire symmetric components. In this case, in line with Eq. (10) the average value of the diagonal elements denotes the isotropic Bloch DMI, while the additional terms responsible for the difference in the diagonal elements denote the anisotropic Bloch DMI. Similarly, we refer to the symmetric off-diagonal components of the DMI matrix as the anisotropic Néel components. For a bilayer system with broken mirror symmetry along the z axis and twofold  $(C_{2v})$  in-plane rotational symmetry, the nonzero DMI tensor elements include  $D_{xx}$ ,  $D_{xy}$ ,  $D_{yx}$ , and  $D_{yy}$ . In this case, the four DMI components are  $D_{iso}^N =$  $(D_{xy} - D_{yx})/2$ ,  $D_{iso}^B = (D_{xx} + D_{yy})/2$ ,  $D_{an}^N = (D_{xy} + D_{yx})/2$ , and  $D_{an}^B = (D_{xx} - D_{yy})/2$ , which in turn give rise to different types of skyrmions. In Figs. 1(a) and 1(b) we show the Néel- and Bloch-type skyrmions, respectively, corresponding to the isotropic Néel and Bloch DMIs. On the other hand, as displayed in Figs. 1(c) and 1(d), the anisotropic and Néel Bloch DMIs [64], which originate from the anisotropy in the planar crystal structure, give rise to antiskyrmions [65] that are related to each other by a 45° in-plane rotation.

### B. Magnon dispersion

Solving the linearized Landau–Lifshitz–Gilbert (LLG) equations of motion, Eqs. (4), for equilibrium magnetization

along z leads to the magnon dispersion,

$$\omega_{\vec{q}} = \frac{\mu_B}{M_{\text{tot}}} \text{Im} \left( J_{\vec{q}}^{xy} - J_{\vec{q}}^{yx} \right) \pm \omega_{\vec{q}}^0, \tag{11}$$

where the first term represents the DMI contribution to the magnonic energy, which is an odd function of  $\vec{q}$ , while the second term is an even function of  $\vec{q}$  and is given by

$$\omega_{\vec{q}}^{0} = \frac{\sqrt{4(J_{\vec{q}}^{xx} - J_{0}^{zz})(J_{\vec{q}}^{yy} - J_{0}^{zz}) - (J_{\vec{q}}^{xy} + J_{\vec{q}}^{yx})^{2}}}{M_{\text{tot}}/\mu_{B}}.$$
 (12)

Similarly, using the equations of motion, Eq. (7), of the micromagnetic model in the continuum limit, the magnon dispersion for a given equilibrium magnetization direction  $\vec{m}_{eq}$  is given by

$$\omega_{\vec{q}} = \frac{4V_M \mu_B}{M_{\text{tot}}} \sum_{\alpha\beta} D_{\alpha\beta} q^{\alpha} m_{\text{eq}}^{\beta} \pm \omega_{\vec{q}}^{0}, \tag{13}$$

where the first term corresponds to the DMI contribution of the magnon energy and the second term is given by

$$\left(\frac{\omega_{\vec{q}}^{0}}{2\mu_{B}V_{M}}\right)^{2} = \left(\vec{H}_{\vec{q}}^{\text{eff}} \cdot \vec{m}_{\text{eq}}\right)^{2} + \sum_{\alpha\beta} \text{adj} \left[\hat{K}_{\vec{q}}^{\text{eff}}\right]_{\alpha\beta} m_{\text{eq}}^{\alpha} m_{\text{eq}}^{\beta} 
- \vec{H}_{\vec{q}}^{\text{eff}} \cdot \vec{m}_{\text{eq}} \sum_{\alpha} \left(K_{\vec{q},\alpha\alpha}^{\text{eff}} - \sum_{\beta} K_{\vec{q},\alpha\beta}^{\text{eff}} m_{\text{eq}}^{\alpha} m_{\text{eq}}^{\beta}\right).$$
(14)

Here,  $adj[\cdots]$  represents the adjoint of the matrix, and

$$\vec{H}_{\vec{q}}^{\text{eff}} \cdot \vec{e}_{\alpha} = \frac{2}{M_{\text{tot}}} \sum_{\beta} \left( A_{\alpha\beta} q_{\beta}^2 m_{\text{eq}}^{\alpha} - K_{\alpha\beta} m_{\text{eq}}^{\beta} \right), \quad (15)$$

$$K_{\bar{q},\alpha\beta}^{\text{eff}} = \frac{2}{M_{\text{tot}}} \sum_{\gamma} \left( A_{\alpha\gamma} q_{\gamma}^2 \delta_{\alpha\beta} - K_{\alpha\beta} \right). \tag{16}$$

The equilibrium magnetization orientation  $\vec{m}_{eq}$  is found by minimizing the magnetic energy of the collinear ferromagnet.

Therefore, the DMI contribution to the magnon energy for any given equilibrium magnetization direction in a system with isotropic crystal structure in the *x-y* plane is given by

$$\omega_{\vec{q}}^{\rm DMI} = \frac{4V_M \mu_B}{M_{\rm tot}} (D^N \vec{e}_z \cdot \vec{q} \times \vec{m}_{\rm eq} + D^B \vec{q} \cdot \vec{m}_{\rm eq}). \tag{17}$$

## C. First-principles calculations of the exchange coupling

We employ the Green's function method to calculate the exchange coupling elements. Within the linear combination of atomic orbitals basis, the multiorbital Hamiltonian  $\hat{H}_{\vec{R}}$  describing the hopping of electrons between two unit cells separated by  $\vec{R}$  is given by

$$\hat{H}_{\vec{R}} = \hat{H}_{\vec{R}}^0 + \hat{H}_{\vec{R}}^{soc} + \hat{\Delta}_{\vec{R}} \hat{\sigma}_z. \tag{18}$$

Here,  $\hat{H}_{\vec{R}}^0$  is the paramagnetic (spin-independent) term,  $\hat{H}_{\vec{R}}^{soc}$  is the SOC term, and  $\hat{\Delta}_{\vec{R}}$  is the exchange splitting matrix responsible for magnetism in the ferromagnet. Note that the SOC and exchange splitting terms are even and odd with respect to time reversal symmetry, respectively.

The effective magnetic field acting on the spin moment of the *i*th ion within a unit cell located at  $\vec{R}$  is given by

$$\vec{B}_{\vec{R},i} = -\left\langle \frac{\partial \hat{\boldsymbol{H}}}{\partial \vec{m}_{\vec{p}}^i} \right\rangle, \tag{19}$$

where  $\langle \cdots \rangle = \int dE \operatorname{Im} \operatorname{Tr}(\cdots \hat{\mathbf{G}}) f(E)/\pi$  is the expectation value and the Hamiltonian matrix elements are given by  $\hat{\mathbf{H}}_{\vec{R},\vec{R}'} = \hat{H}_{\vec{R}-\vec{R}'}$ . The exchange coupling elements entering the magnon dispersion in Eq. (11) are calculated from [66–71]

$$J_0^{i,zz} = -\vec{B}_0^i \cdot \vec{e}_z$$

$$= \int \frac{dE}{\pi} \operatorname{ImTr}([\hat{\Delta G}]_{\vec{R}=0} \hat{\sigma}^z \hat{1}_i) f(E), \qquad (20a)$$

$$J_{\vec{R}}^{ij,\alpha\beta} = -\partial B_0^{i,\alpha} / \partial (\vec{m}_{\vec{R}}^j \cdot \vec{e}_\beta)$$

$$= \int \frac{dE}{\pi} \operatorname{ImTr}([\hat{\Delta G}]_{\vec{R}} \hat{1}_i \hat{\sigma}^\alpha [\hat{\Delta G}]_{-\vec{R}} \hat{\sigma}^\beta \hat{1}_j) f(E). \qquad (20b)$$

Here,  $[\hat{\Delta G}]_{\vec{R}} = \sum_{\vec{k}} \hat{\Delta} \hat{G}_{\vec{k}} e^{-i\vec{k}\cdot\vec{R}}/N_k$ ,  $N_k$  is the number of k points,  $\hat{1}_i$  is the atomic position operator within the unit cell (diagonal matrix elements equal to 1 for atomic orbitals of the ith atom and 0 otherwise), f(E) is the Fermi-Dirac distribution function, and

$$\hat{G}_{\vec{i}} = (E\hat{\mathcal{O}}_{\vec{i}} - \hat{H}_{\vec{i}})^{-1} \tag{21}$$

is the Green's function, where the Fourier transformed Hamiltonian  $\hat{H}_{\vec{k}} = \sum_{\vec{R}} \hat{H}_{\vec{R}} e^{i\vec{k}\cdot\vec{R}}$  and, similarly, the overlap  $\hat{\mathcal{O}}_{\vec{k}}$  matrices are calculated using the linear combination of pseudoatomic orbital approach as implemented in the OPENMX package [72–74].

### III. COMPUTATIONAL DETAILS

The Hamiltonian  $\hat{H}_{\vec{R}}$  and overlap  $\hat{\mathcal{O}}_{\vec{R}}$  matrix elements of the (111) Co/Pt slab consisting of various thicknesses of Co and Pt are determined from density functional theory calculations employing the OPENMX [72–74] *ab initio* package. We adopted Troullier-Martins-type norm-conserving pseudopotentials [75] with partial core correction. We used a  $24 \times 24 \times 1$  k-point mesh for the first Brillouin zone (BZ) integration and an energy cutoff of 500 Ry for numerical integrations in the real-space grid. The localized orbitals were generated with radial cutoffs of 6.0 and 7.0 a.u. for Co and Pt, respectively [72,73]. We used the in-plane lattice parameter a=2.7 Å and the local spin density approximation (LSDA) [76] exchange correlation functional as parameterized by Perdew and Zunger [77].

Structural relaxations were carried using the Vienna Ab initio Simulation Package (VASP) [78,79] within the generalized gradient approximation as parameterized by Perdew *et al.* [80] until the largest atomic force was smaller than 0.01 eV Å<sup>-1</sup>. The pseudopotential and wave functions are treated within the projector augmented-wave method [81,82]. A 15-Å-thick vacuum region is introduced to separate the periodic slabs along the stacking direction. The plane wave cutoff energy was set to 500 eV, and a  $14 \times 14 \times 1$  *k*-point mesh was used in the two-dimensional (2D) BZ sampling.

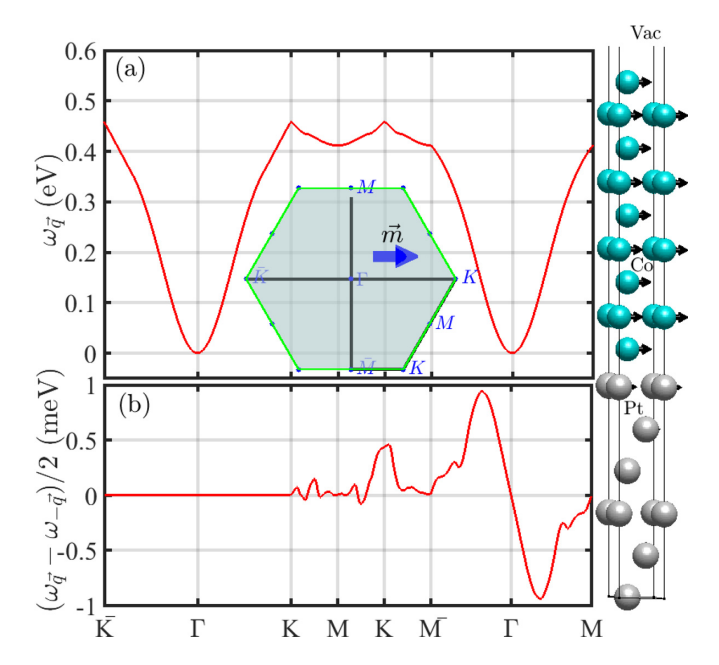


FIG. 2. (a) Magnon dispersion in the spin-spiral regime along high-symmetry directions in the first Brillouin zone, depicted in the inset, for the (111) Co(1.7 nm)/Pt(1.4 nm) bilayer, shown in the right panel, with equilibrium magnetization along the  $\bar{K}$ -K direction. (b) Antisymmetric part of the magnon energy along high-symmetry directions, where a nonzero slope around  $\Gamma$  gives the DMI.

In the calculations of the exchange coupling the energy integration in Eq. (20) was carried out using the Matsubara summation approach with the poles obtained from Ozaki's continued fraction method of the Fermi-Dirac distribution function [83]. The Fermi-Dirac distribution function temperature was set at  $k_BT = 25 \text{ meV}$ , and 60 poles were employed for the Matsubara summation.

## IV. RESULTS AND DISCUSSION

Figure 2(a) shows the magnon dispersion  $\omega_{\vec{q}}$  calculated from Eq. (11) along the high-symmetry directions of the 2D BZ, shown in the inset, for the Pt(1.4 nm)/Co(1.7 nm) bilayer with in-plane magnetization along the  $\bar{K}$ -K direction. The crystal structure is shown on the right side of Fig. 2. According to Eq. (17), the Bloch (Néel) DMI coefficient is given by the slope of  $\omega_{\vec{q}}^{\rm DMI} = (\omega_{\vec{q}} - \omega_{-\vec{q}})/2$  with respect to  $q_y$   $(q_x)$  around the  $\Gamma$  point. Figure 2(b) shows the DMI contribution to the magnon energy along the high-symmetry directions. A finite DMI magnon energy along the  $\bar{M}$ -M path  $\vec{q} \perp \vec{m}_{eq}$  suggests the presence of a nonzero Néel DMI  $\hat{D}^N$ , while the zero slope for the DMI magnon energy around  $\Gamma$  along the  $\vec{q} || \vec{m}$ direction demonstrates the absence of Bloch DMI,  $D^B = 0$ . Figure 3 displays the variation of the ab initio calculated Néel DMI (open blue circles) for the Pt(1.4 nm)/Co( $d_{Co}$ ) bilayer as a function of the inverse Co thickness. The blue line is a linear square fit of the *ab initio* values. We also show for comparison the experimentally reported DMI values (stars and crosses) [54,84–89] of Pt/Co(x)/insulator heterostructures with different insulators. The linear fit, shown by the solid line in Fig. 3, yields an interfacial DMI value of 2.35 pJ/m, which is slightly smaller than the earlier ab initio value of 2.78 pJ/m

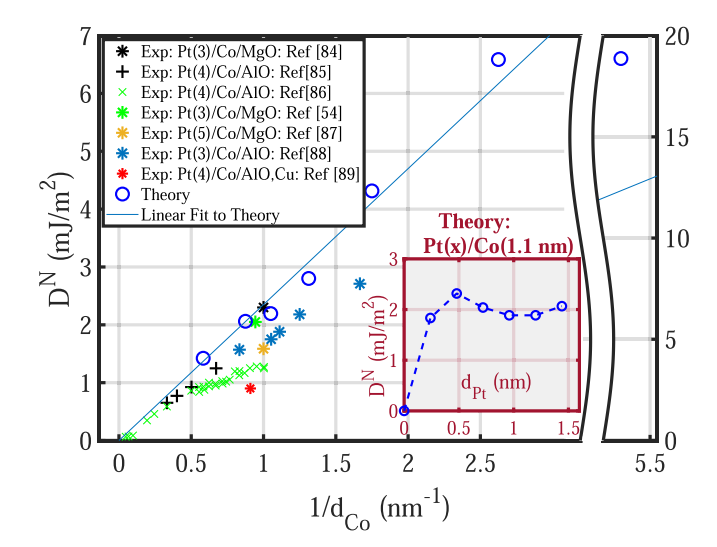


FIG. 3. *Ab initio* Néel DMI (open blue circles) versus inverse Co thicknesses for the (111) Pt (1.4 nm)/Co( $d_{Co}$ ) bilayer slab along with their linear fit (blue line). For comparison we also show the available experimental DMI values (stars and crosses) for various Pt( $d_{Pt}$  nm)/Co(x) bilayers grown on different insulating substrates [54,84–89]. Inset: *Ab initio* Néel DMI versus Pt thicknesses for the Pt( $d_{Pt}$ )/Co(1.1 nm) bilayer.

[90]. The difference can be attributed to the smaller interfacial Co magnetic moment of  $1.8\mu_B$  in this work, compared to the corresponding value of  $1.95\mu_B$  reported in Ref. [90]. Overall, we find relatively good agreement between our results and the experimentally reported data measured at room temperature. It should be noted that a small enhancement of the experimental results is expected due to the oxidation of the interfacial Co atoms with the insulating cap layer [91]. The relatively small overestimation of the theoretical results, which is more significant for thinner Co films, may be attributed to the effect of temperature and the diffusion of atoms near the interface [55,90,92]. The inset shows the dependence of the calculated Néel DMI on the Pt thicknesses for the  $Pt(d_{Pt})/Co(1.1 \text{ nm})$ bilayer, which is relatively weak due to the fact that the interfacial Pt vields the large contributor to the DMI [55]. On the other hand, this result is in contrast to experimental observations [93], in which a diffusionlike dependence of DMI versus Pt thickness has been reported. In view of the interfacial nature of the DMI in heavy-metal/ferromagnet bilayers, it is expected that the interfacial Co atoms experience the dominant contribution of the DMI. From Eq. (8) the DMI for an isotropic bilayer with the magnetization direction along y  $(\vec{m}_{eq}||\vec{e}_{v})$  and magnon propagation along x can be decomposed into its layer- and atom-resolved contributions as follows:

$$D_{R_n}^{N,ij} = \frac{1}{2V_M} \sum_{|\vec{R}| = R_n} J_{\vec{R}}^{ij,zx} (\vec{R} + \vec{r}_i - \vec{r}_j) \cdot \vec{e}_x.$$
 (22)

In the case of the Pt/Co bilayer the atom-resolved DMI can be determined from  $D^{N;i} = \sum_j (D^{N;ij} + D^{N;ji})/2$ , where  $D^{N,ij} = \sum_{R} D^{N;ij}_{R}$ .

Figure 4 shows the layer-resolved DMI versus the layer index of the Pt(1.4 nm)/Co(1.7 nm) bilayer. As expected, we find that the interfacial Co yields the dominant contribution.

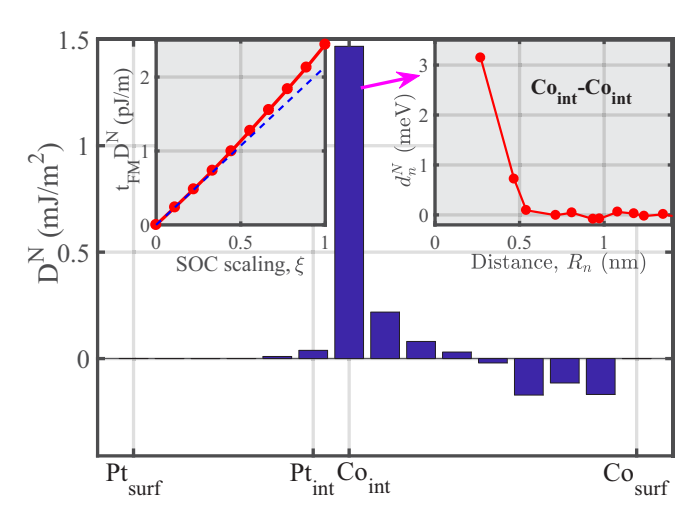


FIG. 4. Layer-resolved Néel DMI for the Pt(1.4 nm)/Co(1.7 nm) bilayer versus the layer index, where Pt<sub>int</sub> and Co<sub>int</sub> denote the interfacial atoms, while Pt<sub>surf</sub> and Co<sub>surf</sub> denote the surface atoms. Left inset: Total interfacial DMI versus the SOC scaling factor, where the dashed line denotes the linear variation of the DMI with SOC. Right inset: Néel DMI for a pair of Co atoms  $d_n^N$  on the interfacial layer versus their interatomic distance  $R_n$ .

One can also determine from Eq. (22) the contribution of the *n*th nearest-neighbor atomic shell to the layer-resolved DMI. Comparing Eq. (22) with Eq. (9) and the corresponding discussion, we obtain

$$d_n^{N,ij} = \frac{4V_M D_{R_n}^{N;ij}}{N_n R_n}. (23)$$

The right inset in Fig. 4 shows the calculated  $d_n^{N,ij}$ , where  $i, j \in \text{Co}_{int}$  lie on the interfacial Co layer. We find that the dominant contribution arises from the first- and, to a lesser extent, second-nearest neighbor atoms. The left inset in Fig. 4 displays the total interfacial DMI for Pt(1.4 nm)/Co(1.7 nm) versus the SOC scaling factor. The small enhancement of the DMI from its linear variation (blue dashed line) for larger

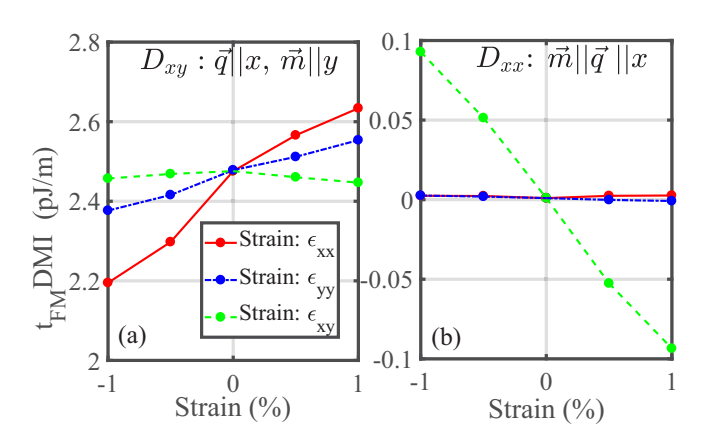


FIG. 5. (a) Interfacial Néel DMI  $D_{xy}$  of the Pt(1.4 nm)/Co(0.6 nm) bilayer for magnon propagation along x and magnetization direction along y versus  $\epsilon_{xx}$ ,  $\epsilon_{xy}$ , and  $\epsilon_{yy}$  strains. (b) Interfacial Bloch DMI  $D_{xx}$  for magnon propagation and magnetization direction along x versus  $\epsilon_{xx}$ ,  $\epsilon_{xy}$ , and  $\epsilon_{yy}$  strains.

TABLE I. Calculated interfacial elasto-DMI coefficients,  $\mathfrak{D}^N_{iso} = \frac{\partial}{\partial \epsilon_{xx}}(D_{xy} - D_{yx})$ ,  $\mathfrak{D}^N_{an} = \frac{\partial}{\partial \epsilon_{xx}}(D_{xy} + D_{yx})$ , and  $\mathfrak{D}^B_{an} = \frac{1}{2}\frac{\partial}{\partial \epsilon_{xy}}D_{xx}$ , for the Pt(1.4 nm)/Co(0.6 nm) and Pt(1.4 nm)/Co(1.1 nm) bilayers, where  $t_{\text{FM}}$  is the thickness of the Co thin film. The values of  $t_{\text{FM}}\mathfrak{D}$  are in units of pJ/m.

	$t_{\mathrm{FM}}\mathfrak{D}^{N}_{iso}$	$t_{\mathrm{FM}}\mathfrak{D}_{\mathrm{an}}^{N}$	$t_{\mathrm{FM}}\mathfrak{D}_{\mathrm{an}}^{B}$
Pt(1.4 nm)/Co(0.6 nm)	38	18	-5
Pt(1.4 nm)/Co(1.1 nm)	52	14	-8

SOC values is due to the contributions from higher-order terms in SOC.

Finally, we have investigated the effect of strain on the DMI for various Pt and Co thicknesses. In the presence of strain  $\epsilon_{ij}$ , the modified primitive lattice vectors  $\vec{a}'_i$  are given by  $(\vec{a}'_i - \vec{a}_i) \cdot \vec{e}_j = \sum_k \epsilon_{kj} \vec{a}_i \cdot \vec{e}_k$ , where the  $\vec{e}_j$ 's represent the unit vectors in Cartesian coordinates. Note that in Voigt notation the off-diagonal elements of the strain matrix  $\epsilon_{i \neq j}$  should be divided by 2 to avoid double counting [94,95]. Figures 5(a) and 5(b) show the Néel,  $D_{yx}$ , and Bloch,  $D_{xx}$ , DMIs, respectively, multiplied by the thickness of the Co film, versus  $\epsilon_{xx}$ ,  $\epsilon_{yy}$ , and  $\epsilon_{xy}$  for the Pt(1.4 nm)/Co(0.6 nm) bilayer. We observe that under shear strain  $\epsilon_{xy}$  nonvanishing *anisotropic* Bloch (diagonal) DMI components,  $D_{xx} = -D_{yy}$ , emerge, while the Néel DMI  $(D_{xy}, D_{yx})$  remains intact.

We have derived a general expression for the strain-induced change in the DMI given by

$$\delta D_{\alpha\beta} = \left[ \frac{\epsilon_{\alpha\alpha} - \epsilon_{\beta\beta}}{2} \mathfrak{D}_{\text{an}}^{N} + \frac{\epsilon_{\alpha\alpha} + \epsilon_{\beta\beta}}{2} \mathfrak{D}_{iso}^{N} \right] \vec{e}_{z} \cdot \vec{e}_{\alpha} \times \vec{e}_{\beta}$$
$$-2 \mathfrak{D}_{\text{an}}^{B} \sum_{\alpha' \neq \alpha} \epsilon_{\alpha\alpha'} \vec{e}_{z} \cdot \vec{e}_{\alpha'} \times \vec{e}_{\beta}, \tag{24}$$

where the elasto-DMI coefficients are calculated from  $\mathfrak{D}_{iso}^N = \frac{\partial}{\partial \epsilon_{xx}}(D_{xy} - D_{yx}), \, \mathfrak{D}_{an}^N = \frac{\partial}{\partial \epsilon_{xx}}(D_{xy} + D_{yx}), \, \text{and} \, \mathfrak{D}_{an}^B = \frac{1}{2} \frac{\partial}{\partial \epsilon_{xy}} D_{xx}.$  In Table I, we list the values of the elasto-DMI coefficients for the Pt(1.4 nm)/Co(0.6 nm) and Pt(1.4 nm)/Co(1.1 nm) bilayers. The results show a larger modulation of the isotropic DMI

 $\mathfrak{D}_{iso}^N$  under strain. The calculated elasto-DMI coefficients are about 5 times smaller than the recently reported experimental values which lie in the range of 200–300 pJ/m [51]. However, since the experimental data correspond to a Pt/Co/Pt trilayer device which relies on the different qualities of the two Pt/Co interfaces to break the mirror symmetry, a direct comparison with our *ab initio* results may not be appropriate. Note that in polycrystalline systems an averaging of the anisotropic Bloch,  $\mathfrak{D}_{an}^B$ , and Néel,  $\mathfrak{D}_{an}^N$ , components is expected. The opposite signs of the anisotropic DMI under shear strain  $\epsilon_{xy}$  compared to  $\epsilon_{xx}$  result in their cancellation in the polycrystalline Pt/Co bilayers.

### V. CONCLUSIONS

In summary, we have presented an accurate and computationally efficient approach to calculate the DMI from first-principles calculations. The approach was applied to the (111) Pt/Co bilayer where the DMI was calculated for various thicknesses of the Co and Pt thin films. Overall, the ab initio results are in relatively good agreement with a wide range of experiments on different insulating substrates. The atomresolved DMI suggests that the nearest-neighbor interfacial Co atoms yield the largest contribution to the DMI. We have also investigated the modulation of the DMI under various types of strain which in turn gives rise to large anisotropic DMI components. We find large changes in the isotropic DMI component under  $\epsilon_{\alpha\alpha}$  ( $\alpha=x,y$ ) strain. The strain-induced control of DMI in multiferroic devices may pave an efficient way for skyrmion and domain-wall-motion-based spintronic applications.

### ACKNOWLEDGMENTS

The work is supported by NSF ERC-Translational Applications of Nanoscale Multiferroic Systems (TANMS) Grant No. 1160504, NSF PFI-RP Grant No. 1919109, and NSF Partnership in Research and Education in Materials (PREM) Grant No. DMR-1828019.

<sup>[1]</sup> A. Fert, V. Cros, J. Sampaio, Skyrmions on the track, Nat. Nanotechnol. **8**, 152 (2013).

<sup>[2]</sup> N. S. Kiselev, A. N. Bogdanov, R. Schäfer, and U. K. RöBler, Chiral skyrmions in thin magnetic films: New objects for magnetic storage technologies? J. Phys. D 44, 392001 (2011).

<sup>[3]</sup> N. Nagaosa and Y. Tokura, Topological properties and dynamics of magnetic skyrmions, Nat. Nanotechnol. **8**, 899 (2013).

<sup>[4]</sup> A. N. Bogdanov and D. A. Yablonskii, Thermodynamically stable vortices in magnetically ordered crystals. The mixed state of magnets, Zh. Eksp. Teor. Fiz. 95, 178 (1989) [Sov. Phys. JETP 68, 101 (1989)].

<sup>[5]</sup> A. Bogdanov and A. Hubert, Thermodynamically stable magnetic vortex states in magnetic crystals, J. Magn. Magn. Mater. 138, 255 (1994).

<sup>[6]</sup> S. Mühlbauer, B. Binz, F. Jonietz, C. Pfleiderer, A. Rosch, A. Neubauer, R. Georgii, and P. Böni, Skyrmion lattice in a chiral magnet, Science 323, 915 (2009).

<sup>[7]</sup> X. Z. Yu, Y. Onose, N. Kanazawa, J. H. Park, J. H. Han, Y. Matsui, N. Nagaosa, and Y. Tokura, Real-space observation of a two-dimensional skyrmion crystal, Nature (London) 465, 901 (2010).

<sup>[8]</sup> X. Z. Yu, N. Kanazawa, Y. Onose, K. Kimoto, W. Z. Zhang, S. Ishiwata, Y. Matsui, and Y. Tokura, Near room-temperature formation of a skyrmion crystal in thin-films of the helimagnet FeGe, Nat. Mater. 10, 106 (2011).

<sup>[9]</sup> K. Shibata, X. Z. Yu, T. Hara, D. Morikawa, N. Kanazawa, K. Kimoto, S. Ishiwata, Y. Matsui, and Y. Tokura, Towards control of the size and helicity of skyrmions in helimagnetic alloys by spin-orbit coupling, Nat. Nanotechnol. 8, 723 (2013).

<sup>[10]</sup> A. Fert, N. Reyren, and V. Cros, Magnetic skyrmions: Advances in physics and potential applications, Nat. Rev. Mater. 2, 17031 (2017).

<sup>[11]</sup> K. Everschor-Sitte, J. Masell, R. M. Reeve, and M. Kläui, Perspective: Magnetic skyrmions-Overview of recent progress

- in an active research field, J. Appl. Phys. **124**, 240901 (2018).
- [12] G. Finocchio, F. Büttner, R. Tomasello, M. Carpentieri, and M. Kläui, Magnetic skyrmions: From fundamental to applications, J. Phys. D 49, 423001 (2016).
- [13] W. Jiang, P. Upadhyaya, W. Zhang, G. Yu, M. B. Jungfleisch, F. Y. Fradin, J. E. Pearson, Y. Tserkovnyak, K. L. Wang, O. Heinonen, S. G. E. te Velthuis, and A. Hoffmann, Blowing magnetic skyrmion bubbles, Science 349, 283 (2015).
- [14] A. Hrabec, J. Sampaio, M. Belmeguenai, I. Gross, R. Weil, S. M. Chérif, A. Stashkevich, V. Jacques, A. Thiaville, and S. Rohart, Current-induced skyrmion generation and dynamics in symmetric bilayers, Nat. Commun. 8, 15765 (2017).
- [15] J. Sampaio, V. Cros, S. Rohart, A. Thiaville, and A. Fert, Nucleation, stability and current-induced motion of isolated magnetic skyrmions in nanostructures, Nat. Nanotechnol. 8, 839 (2013).
- [16] G. Yu, P. Upadhyaya, X. Li, W. Li, S. K. Kim, Y. Fan, K. L. Wong, Y. Tserkovnyak, P. K. Amiri, and K. L. Wang, Room-temperature creation and spin-orbit torque manipulation of skyrmions in thin films with engineered asymmetry, NanoLett. 16, 1981 (2016).
- [17] F. Büttner, I. Lemesh, M. Schneider, B. Pfau, C. M. Günther, P. Hessing, J. Geilhufe, L. Caretta, D. Engel, B. Krüger, J. Viefhaus, S. Eisebitt, and G. S. D. Beach, Field-free deterministic ultrafast creation of magnetic skyrmions by spin-orbit torques, Nat. Nanotechnol. 12, 1040 (2017).
- [18] F. Hellman *et al.*, Interface-induced phenomena in magnetism, Rev. Mod. Phys. 89, 025006 (2017).
- [19] A. Soumyanarayanan, M. Raju, A. L. Gonzalez Oyarce, A. K. C. Tan, M.-Y. Im, A. P. Petrović, P. Ho, K. H. Khoo, M. Tran, C. K. Gan, F. Ernult, and C. Panagopoulos, Tunable room-temperature magnetic skyrmions in Ir/Fe/Co/Pt multilayers, Nat. Mater. 16, 898 (2017).
- [20] I. J. Dzyaloshinsky, A thermodynamic theory of "weak" ferromagnetism of antiferromagnetics, Phys. Chem. Solids 4, 241 (1958).
- [21] T. Moriya, Anisotropic Superexchange Interaction and Weak Ferromagnetism, Phys. Rev. 120, 91 (1960)
- [22] L. Udvardi and L. Szunyogh, Chiral Asymmetry of the Spin-Wave Spectra in Ultrathin Magnetic Films, Phys. Rev. Lett. 102, 207204 (2009).
- [23] A. T. Costa, R. B. Muniz, S. Lounis, A. B. Klautau, and D. L. Mills, Spin-orbit coupling and spin waves in ultrathin ferromagnets: The spin-wave Rashba effect, Phys. Rev. B 82, 014428 (2010).
- [24] J. H. Moon, S. M. Seo, K. J. Lee, K. W. Kim, J. Ryu, H. W. Lee, R. D. McMichael, and M. D. Stiles, Spin-wave propagation in the presence of interfacial Dzyaloshinskii-Moriya interaction, Phys. Rev. B 88, 184404 (2013).
- [25] A. F. Volkov, F. S. Bergeret, and K. B. Efetov, Spin polarization and orbital effects in superconductor-ferromagnet structures, Phys. Rev. B 99, 144506 (2019).
- [26] K. Di, V. L. Zhang, H. S. Lim, S. C. Ng, M. H. Kuok, J. Yu, J. Yoon, X. Qiu, and H. Yang, Direct Observation of the Dzyaloshinskii-Moriya Interaction in a Pt/Co/Ni Film, Phys. Rev. Lett. 114, 047201 (2015).
- [27] X. Ma, G. Yu, X. Li, T. Wang, D. Wu, K. S. Olsson, Z. Chu, K. An, J. Q. Xiao, K. L. Wang, and X. Li, Interfacial control of Dzyaloshinskii-Moriya interaction in heavy

- metal/ferromagnetic metal thin film heterostructures, Phys. Rev. B **94**, 180408(R) (2016).
- [28] X. Ma, G. Yu, S. A. Razavi, S. S. Sasaki, X. Li, K. Hao, S. H. Tolbert, K. L. Wang, and X. Li, Dzyaloshinskii-Moriya Interaction across an Antiferromagnet-Ferromagnet Interface, Phys. Rev. Lett. 119, 027202 (2017).
- [29] K.-W. Kim, K.-W. Moon, N. Kerber, J. Nothhelfer, and K. Everschor-Sitte, Asymmetric skyrmion Hall effect in systems with a hybrid Dzyaloshinskii-Moriya interaction, Phys. Rev. B 97, 224427 (2018).
- [30] H. Yang, G. Chen, A. A. C. Cotta, A. T. N'Diaye, S. A. Nikolaev, E. A. Soares, W. A. A. Macedo, K. Liu, A. K. Schmid, A. Fert, and M. Chshiev, Significant Dzyaloshinskii-Moriya interaction at graphene-ferromagnet interfaces due to the Rashba effect, Nat. Mater. 17, 605 (2018).
- [31] A. Manchon, H. C. Koo, J. Nitta, S. Frolov, and R. Duine, New perspectives for Rashba spin-orbit coupling, Nat. Mater. 14, 871 (2015).
- [32] I. Kézsmárki, S. Bordács, P. Milde, E. Neuber, L. M. Eng, J. S. White, H. M. Rønnow, C. D. Dewhurst, M. Mochizuki, K. Yanai, H. Nakamura, D. Ehlers, V. Tsurkan, and A. Loidl, Néeltype skyrmion lattice with confined orientation in the polar magnetic semiconductor GaV<sub>4</sub>S<sub>8</sub>, Nat. Mater. 14, 1116 (2015).
- [33] T. Kurumaji, T. Nakajima, V. Ukleev, A. Feoktystov, T.-h. Arima, K. Kakurai, and Y. Tokura, Néel-type skyrmion lattice in the tetragonal polar magnet VOSe<sub>2</sub>O<sub>5</sub>, Phys. Rev. Lett. 119, 237201 (2017).
- [34] S. Seki, X. Yu, S. Ishiwata, and Y. Tokura, Observation of skyrmions in a multiferroic material, Science 336, 198 (2012).
- [35] G. Finocchio, M. Di Ventra, K. Y. Camsari, K. Everschor-Sitte, P. K. Amiri, and Z. Zeng, The promise of spintronics for unconventional computing, J. Magn. Magn. Mater. 521, 167506 (2021).
- [36] R. Tomasello, E. Martinez, R. Zivieri, L. Torres, M. Carpentieri, and G. Finocchio, A strategy for the design of skyrmion race-track memories, Sci. Rep. 4, 6784 (2014).
- [37] W. Kang, Y. Huang, C. Zheng, W. Lv, N. Lei, Y. Zhang, X. Zhang, Y. Zhou, and W. Zhao, Voltage controlled magnetic skyrmion motion for racetrack memory, Sci. Rep. 6, 23164 (2016).
- [38] X. Zhang, Y. Zhou, M. Ezawa, G. P. Zhao, and W. Zhao, Magnetic skyrmion transistor: Skyrmion motion in a voltage-gated nanotrack, Sci. Rep. 5, 11369 (2015).
- [39] X. Zhang, M. Ezawa, and Y. Zhou, Magnetic skyrmion logic gates: Conversion, duplication and merging of skyrmions, Sci. Rep. 5, 9400 (2015).
- [40] G. Finocchio, M. Ricci, R. Tomasello, A. Giordano, M. Lanuzza, V. Puliafito, P. Burrascano, B. Azzerboni, and M. Carpentieri, Skyrmion based microwave detectors and harvesting, Appl. Phys. Lett. 107, 262401 (2015).
- [41] Z. He and D. Fan, A tunable magnetic skyrmion neuron cluster for energy efficient artificial neural network, in 2017 Design, Automation, Test in Europe Conference, Exhibition (DATE), Lausanne (IEEE, Piscataway, NJ, 2017), pp. 350–355.
- [42] S. Li, W. Kang, X. Chen, J. Bai, B. Pan, Y. Zhang, and W. Zhao, Emerging neuromorphic computing paradigms exploring magnetic skyrmions, in 2018 IEEE Computer Society Annual Symposium on VLSI (ISVLSI),

- Hong Kong, China (IEEE, Piscataway, NJ, 2018), pp. 539–544.
- [43] N. Romming, A. Kubetzka, C. Hanneken, K. von Bergmann, and R. Wiesendanger, Field-Dependent Size and Shape of Single Magnetic Skyrmions, Phys. Rev. Lett. 114, 177203 (2015).
- [44] W. Koshibae and N. Nagaosa, Creation of skyrmions and antiskyrmions by local heating, Nat. Commun. 5, 5148 (2014).
- [45] J. Rowland, S. Banerjee, and M. Randeria, Skyrmions in chiral magnets with Rashba and Dresselhaus spin-orbit coupling, Phys. Rev. B 93, 020404(R) (2016).
- [46] S. A. Díaz and R. E. Troncoso, Controlling skyrmion helicity via engineered Dzyaloshinskii-Moriya interactions, J. Phys.: Condens. Matter 28, 426005 (2016).
- [47] J. Masell and K. Everschor-Sitte, Current-induced dynamics of chiral magnetic structures: creation, motion, and applications, arXiv:2004.13535.
- [48] T. Koyama, Y. Nakatani, J. Ieda, and D. Chiba, Electric field control of magnetic domain wall motion via modulation of the Dzyaloshinskii-Moriya interaction, Sci. Adv. 4, eaav0265 (2018).
- [49] W. Zhang, H. Zhong, R. Zang, Y. Zhang, S. Yu, G. Han, G. L. Liu, S. S. Yan, S. Kang, and L. M. Mei, Electrical field enhanced interfacial Dzyaloshinskii-Moriya interaction in MgO/Fe/Pt system, Appl. Phys. Lett. 113, 122406 (2018).
- [50] T. Srivastava, M. Schott, R. Juge, V. Křižáková, M. Belmeguenai, Y. Roussigné, A. Bernand-Mantel, L. Ranno, S. Pizzini, S.-M. Chérif, A. Stashkevich, S. Auffret, O. Boulle, G. Gaudin, M. Chshiev, C. Baraduc, and H. Béa, Large-Voltage Tuning of Dzyaloshinskii-Moriya Interaction: A Route toward Dynamic Control of Skyrmion Chirality, Nano Lett. 18, 4871 (2018).
- [51] N. S. Gusev, A. V. Sadovnikov, S. A. Nikitov, M. V. Sapozhnikov, and O. G. Udalov, Manipulation of the Dzyaloshinskii-Moriya Interaction in Co/Pt Multilayers with Strain, Phys. Rev. Lett. 124, 157202 (2020).
- [52] S. Woo, K. Litzius, B. Krüger, M.-Y. Im, L. Caretta, K. Richter, M. Mann, A. Krone, R. M. Reeve, M. Weigand, P. Agrawal, I. Lemesh, M.-A. Mawass, P. Fischer, M. Kläui, and G. S. D. Beach, Observation of room-temperature magnetic skyrmions and their current-driven dynamics in ultrathin metallic ferromagnets, Nat. Mater. 15, 501 (2016).
- [53] C. Moreau-Luchaire, C. Moutafis, N. Reyren, J. Sampaio, C. A. F. Vaz, N. Van Horne, K. Bouzehouane, K. Garcia, C. Deranlot, P. Warnicke, P. Wohlhüter, J.-M. George, M. Weigand, J. Raabe, V. Cros, and A. Fert, Additive interfacial chiral interaction in multilayers for stabilization of small individual skyrmions at room temperature, Nat. Nanotechnol. 11, 444 (2016)
- [54] O. Boulle, J. Vogel, H. Yang, S. Pizzini, D. de Souza Chaves, A. Locatelli, T. Onur Menteş, A. Sala, L. D. Buda-Prejbeanu, O. Klein, M. Belmeguenai, Y. Roussigné, A. Stashkevich, S. Mourad Chérif, L. Aballe, M. Foerster, M. Chshiev, S. Auffret, I. Mihai Miron, and G. Gaudin, Room-temperature chiral magnetic skyrmions in ultrathin magnetic nanostructures, Nat. Nanotechnol. 11, 449 (2016).
- [55] H. Yang, A. Thiaville, S. Rohart, A. Fert, and M. Chshiev, Anatomy of Dzyaloshinskii-Moriya Interaction at Co/Pt Interfaces, Phys. Rev. Lett. 115, 267210 (2015).
- [56] B. Zimmermann, G. Bihlmayer, M. Böttcher, M. Bouhassoune, S. Lounis, J. Sinova, S. Heinze, S. Blügel, and B. Dupe,

- Comparison of first-principles methods to extract magnetic parameters in ultrathin films: Co/Pt(111), Phys. Rev. B **99**, 214426 (2019).
- [57] S. Mankovsky and H. Ebert, Accurate scheme to calculate the interatomic Dzyaloshinskii-Moriya interaction parameters, Phys. Rev. B **96**, 104416 (2017).
- [58] F. Freimuth, S. Blügel, and Y. Mokrousov, Relation of the Dzyaloshinskii-Moriya interaction to spin currents and to the spin-orbit field, Phys. Rev. B 96, 054403 (2017).
- [59] N. Kato, M. Kawaguchi, Y.-C. Lau, T. Kikuchi, Y. Nakatani, and M. Hayashi, Current-Induced Modulation of the Interfacial Dzyaloshinskii-Moriya Interaction, Phys. Rev. Lett. 122, 257205 (2019).
- [60] H. Yang, O. Boulle, V. Cros, A. Fert, and M. Chshiev, Controlling Dzyaloshinskii-Moriya interaction via chirality dependent atomic-layer stacking, insulator capping and electric field, Sci. Rep. 8, 12356 (2018).
- [61] C. Deger, Strain-enhanced Dzyaloshinskii-Moriya interaction at Co/Pt interfaces, Sci. Rep. **10**, 12314 (2020).
- [62] O. G. Udalov and I. S. Beloborodov, Strain-dependent Dzyaloshinskii-Moriya interaction in a ferromagnet/heavymetal bilayer, Phys. Rev. B 102, 134422 (2020).
- [63] I. A. Ado, A. Qaiumzadeh, A. Brataas, and M. Titov, Chiral ferromagnetism beyond Lifshitz invariants, Phys. Rev. B 101, 161403(R) (2020).
- [64] L. Camosi, S. Rohart, O. Fruchart, S. Pizzini, M. Belmeguenai, Y. Roussigné, A. Stashkevich, S. M. Cherif, L. Ranno, M. de Santis, and J. Vogel, Anisotropic Dzyaloshinskii-Moriya Interaction in ultra-thin epitaxial Au/Co/W(110), Phys. Rev. B 95, 214422 (2017)
- [65] M. Hoffmann, B. Zimmermann, G. P. Müller, D. Schürhoff, N. S. Kiselev, C. Melcher, and S. Blugel, Antiskyrmions stabilized at interfaces by anisotropic Dzyaloshinskii-Moriya interactions, Nat. Commun. 8, 308 (2017).
- [66] A. I. Liechtenstein, M. I. Katsnelson, V. P. Antropov, and V. A. Gubanova, Local spin density functional approach to the theory of exchange interactions in ferromagnetic metals and alloys, J. Magn. Magn. Mater. 67, 65 (1987).
- [67] M. I. Katsnelson and A. I. Lichtenstein, First-principles calculations of magnetic interactions in correlated systems, Phys. Rev. B 61, 8906 (2000).
- [68] L. Udvardi, L. Szunyogh, K. Palotás, and P. Weinberger, First-principles relativistic study of spin waves in thin magnetic films, Phys. Rev. B 68, 104436 (2003).
- [69] H. Ebert and S. Mankovsky, Anisotropic exchange coupling in diluted magnetic semiconductors: *Ab initio* spin-density functional theory, Phys. Rev. B **79**, 045209 (2009).
- [70] Y. O. Kvashnin, A. Bergman, A. I. Lichtenstein, and M. I. Katsnelson, Relativistic exchange interactions in  $CrX_3$  (X = Cl, Br, I) monolayers, Phys. Rev. B **102**, 115162 (2020).
- [71] A. Secchi, A. Lichtenstein, and M. Katsnelson, Magnetic interactions in strongly correlated systems: Spin and orbital contributions, Ann. Phys. (NY) **360**, 61 (2015).
- [72] T. Ozaki, Variationally optimized atomic orbitals for large-scale electronic structures, Phys. Rev. B 67, 155108 (2003).
- [73] T. Ozaki and H. Kino, Numerical atomic basis orbitals from H to Kr, Phys. Rev. B **69**, 195113 (2004).
- [74] T. Ozaki and H. Kino, Efficient projector expansion for the ab initio LCAO method, Phys. Rev. B 72, 045121 (2005).

- [75] N. Troullier and J. L. Martins, Efficient pseudopotentials for plane-wave calculations, Phys. Rev. B 43, 1993 (1991).
- [76] D. M. Ceperley and B. J. Alder, Ground State of the Electron Gas by a Stochastic Method, Phys. Rev. Lett. 45, 566 (1980).
- [77] J. P. Perdew and A. Zunger, Self-interaction correction to density-functional approximations for many-electron systems, Phys. Rev. B 23, 5048 (1981).
- [78] G. Kresse and J. Furthmüller, Efficient iterative schemes for ab initio total-energy calculations using a plane-wave basis set, Phys. Rev. B 54, 11169 (1996).
- [79] G. Kresse and J. Furthmüller, Efficiency of *ab-initio* total energy calculations for metals and semiconductors using a plane-wave basis set, Comput. Mater. Sci. 6, 15 (1996).
- [80] J. P. Perdew, K. Burke, and M. Ernzerhof, Generalized Gradient Approximation Made Simple, Phys. Rev. Lett. 77, 3865 (1996).
- [81] G. Kresse and D. Joubert, From ultrasoft pseudopotentials to the projector augmented-wave method, Phys. Rev. B 59, 1758 (1999).
- [82] P. E. Blöchl, Projector augmented-wave method, Phys. Rev. B 50, 17953 (1994).
- [83] T. Ozaki, Continued fraction representation of the Fermi-Dirac function for large-scale electronic structure calculations, Phys. Rev. B 75, 035123 (2007).
- [84] A. Cao, X. Zhang, B. Koopmans, S. Peng, Y. Zhang, Z. Wang, S. Yan, H. Yang, and W. Zhao, Tuning the Dzyaloshinskii-Moriya interaction in Pt/Co/MgO heterostructures through the MgO thickness, Nanoscale 10, 12062 (2018).
- [85] J. Cho, N.-H. Kim, J. Jung, D.-S. Han, H. J. M. Swagten, J.-S. Kim, and C.-Y. You, Thermal annealing effects on the interfacial Dzyaloshinskii-Moriya interaction energy density and perpendicular magnetic anisotropy, IEEE Trans. Magn. 54, 1500104 (2018).
- [86] J. Cho, N.-H. Kim, S. Lee, J.-S. Kim, R. Lavrijsen, A. Solignac, Y. Yin, D.-S. Han, N. J. J. van Hoof, H. J. M. Swagten, B. Koopmans, and C.-Y. You, Thickness dependence of the interfacial Dzyaloshinskii-Moriya interaction in inversion symmetry broken systems, Nat. Commun. 6, 7635 (2015).

- [87] X. Ma, G. Yu, C. Tang, X. Li, C. He, J. Shi, K. L. Wang, and X. Li, Interfacial Dzyaloshinskii-Moriya Interaction: Effect of 5d Band Filling and Correlation with Spin Mixing Conductance, Phys. Rev. Lett. 120, 157204 (2018).
- [88] M. Belmeguenai, J.-P. Adam, Y. Roussigné, S. Eimer, T. Devolder, J.-V. Kim, S. M. Cherif, A. Stashkevich, and A. Thiaville, Interfacial Dzyaloshinskii-Moriya interaction in perpendicularly magnetized Pt/Co/AlO<sub>x</sub> ultrathin films measured by Brillouin light spectroscopy, Phys. Rev. B 91, 180405(R) (2015).
- [89] N.-H. Kim, J. Cho, J. Jung, D.-S. Han, Y. Yin, J.-S. Kim, H. J. M. Swagten, K. Lee, M.-H. Jung, and C.-Y. You, Role of top and bottom interfaces of a Pt/Co/AlOx system in Dzyaloshinskii-Moriya interaction, interface perpendicular magnetic anisotropy, and magneto-optical Kerr effect, AIP Adv. 7, 035213 (2017).
- [90] B. Zimmermann, W. Legrand, D. Maccariello, N. Reyren, V. Cros, S. Blügel, and A. Fert, Dzyaloshinskii-Moriya interaction at disordered interfaces from *ab initio* theory: Robustness against intermixing and tunability through dusting, Appl. Phys. Lett. 113, 232403 (2018).
- [91] H. T. Nembach, E. Jue, E. R. Evarts, and J. M. Shaw, Correlation between Dzyaloshinskii-Moriya interaction and orbital angular momentum at an oxide-ferromagnet interface, Phys. Rev. B 101, 020409(R) (2020).
- [92] A. W. J. Wells, P. M. Shepley, C. H. Marrows, and T. A. Moore, Effect of interfacial intermixing on the Dzyaloshinskii-Moriya interaction in Pt/Co/Pt, Phys. Rev. B 95, 054428 (2017).
- [93] S. Tacchi, R. E. Troncoso, M. Ahlberg, G. Gubbiotti, M. Madami, J. Akerman, and P. Landeros, Interfacial Dzyaloshinskii-Moriya Interaction in Pt/CoFeB Films: Effect of the Heavy-Metal Thickness, Phys. Rev. Lett. 118, 147201 (2017).
- [94] D. Iotova, N. Kioussis, and S. P. Lim, Electronic structure and elastic properties of the  $Ni_3X$  (X = Mn, Al, Ga, Si, Ge) intermetallics, Phys. Rev. B **54**, 14413 (1996).
- [95] F. Mahfouzi, G. P. Carman, and N. Kioussis, Magnetoelastic and magnetostrictive properties of Co<sub>2</sub>XAl Heusler compounds, Phys. Rev. B 102, 094401 (2020).